Title
Tracking the Chemical and Structural Evolution of the TiS2 Electrode in the Lithium-Ion Cell Using Operando X-ray Absorption Spectroscopy

Journal
Nano Letters, 18(7)

ISSN
1530-6984

Authors
Zhang, Liang
Sun, Dan
Kang, Jun
et al.

Publication Date
2018-07-11

DOI
10.1021/acs.nanolett.8b01680

Peer reviewed

NANO LETTERS
Cite This: Nano Lett. XXXX, XXX, XXX−XXX
Letter
pubs.acs.org/NanoLett

Tracking the Chemical and Structural Evolution of the TiS_2 Electrode in the Lithium-Ion Cell Using Operando X-ray Absorption Spectroscopy

Liang Zhang,[†] Dan Sun,[‡] Jun Kang,[§] Hsiao-Tsu Wang,[∥] Shang-Hsien Hsieh,[†,⊥] Way-Faung Pong,[⊥] Hans A. Bechtel,[†] Jun Feng,[†] Lin-Wang Wang,[§] Elton J. Cairns,[‡,#] and Jinghua Guo*[,†,▽]

[†]Advanced Light Source, [‡]Energy Storage and Distributed Resources Division, and [§]Material Sciences Division, Lawrence Berkeley National Laboratory, Berkeley, California 94720, United States

[∥]Department of Physics, National Tsing Hua University, Hsinchu 30013, Taiwan

[⊥]Department of Physics, Tamkang University, Tamsui 251, Taiwan

[#]Department of Chemical and Biomolecular Engineering, University of California, Berkeley, California 94720, United States

[▽]Department of Chemistry and Biochemistry, University of California, Santa Cruz, California 95064, United States

Supporting Information

ABSTRACT: As the lightest and cheapest transition metal dichalcogenide, TiS_2 possesses great potential as an electrode material for lithium batteries due to the advantages of high energy density storage capability, fast ion diffusion rate, and low volume expansion. Despite the extensive investigation of its electrochemical properties, the fundamental discharge−charge reaction mechanism of the TiS_2 electrode is still elusive. Here, by a combination of ex situ and operando X-ray absorption spectroscopy with density functional theory calculations, we have clearly elucidated the evolution of the structural and chemical properties of TiS_2 during the discharge−charge processes. The lithium intercalation reaction is highly reversible and both Ti and sulfur are involved in the redox reaction during the discharge and charge processes. In contrast, the conversion reaction of TiS_2 is partially reversible in the first cycle. However, Ti—O related compounds are developed during electrochemical cycling over extended cycles, which results in the decrease of the conversion reaction reversibility and the rapid capacity fading. In addition, the solid electrolyte interphase formed on the electrode surface is found to be highly dynamic in the initial cycles and then gradually becomes more stable upon further cycling. Such understanding is important for the future design and optimization of TiS_2 based electrodes for lithium batteries.

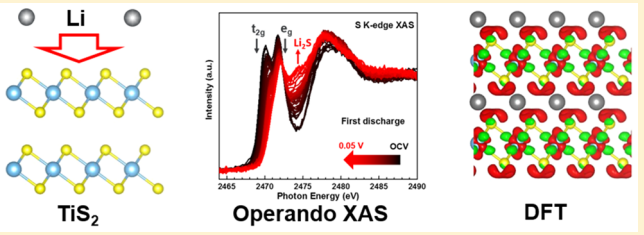

KEYWORDS: *Lithium ion batteries, TiS_2, electronic structure, in situ and operando, X-ray absorption spectroscopy*

Developing electrical energy storage systems with high energy density and low cost is vitally important for powering our future society. Lithium-ion batteries (LIBs) are the dominant energy storage devices and have been widely used in portable electronic devices and electric vehicles.[1−3] However, the specific capacities of the conventional electrode materials for LIBs are approaching their theoretical limits, and therefore, developing new high-energy electrode materials is essential. Transition metal dichalcogenides (TMDs) are promising candidates for next-generation high-energy rechargeable LIBs, which have shown great potential mainly due to the advantages of their unique layered structure, high electronic conductivity, and high theoretical specific capacity.[4−6] Among all the TMDs, TiS_2 is the lightest and least expensive, accompanied by the benefits of highest energy density storage capability and low volume change during the discharge/charge process.

The pioneering work by Whittingham on the concept of intercalation electrodes revealed TiS_2 to be a very stable and high-capacity electrode material with a long cycle life.[7] However, Li/TiS_2 cells suffered irreversible changes mainly due to the safety problem caused by lithium dendrite formation in liquid electrolytes, which limited the real application of this material.[8] The introduction of layered metal oxides by Goodenough and the development of LIBs by the Sony company in the 1990s resulted in a loss of interest in the use of TiS_2 as an electrode.[3,9] Nonetheless, the recent revival of interest in lithium metal chemistry has motivated researchers to reexamine the TiS_2 electrode.[2,10−15]

The average discharge voltage of the TiS_2 electrode is ∼2.1 V versus Li/Li^+ when used as the lithium intercalation host and a 100% utilization of TiS_2 can result in a specific energy of ∼450 Wh/kg by combining with a metallic lithium negative electrode.[9,16] Because of the relatively high discharge voltage, TiS_2 is mostly used as the cathode material[14,15,17,18] but a few

Received: April 25, 2018
Revised: May 15, 2018
Published: June 1, 2018

DOI: 10.1021/acs.nanolett.8b01680
Nano Lett. XXXX, XXX, XXX−XXX

reports are also available where it is used as the anode material for LIBs.[19−21] Although the electrochemical properties of TiS_2 have been extensively investigated since its inception as a promising electrode material,[7,9,22−24] the detailed lithiation and delithiation mechanism of TiS_2, especially the chemical and structural evolution during cycling, is still missing, which is of great significance for developing novel concepts to modify the structure of TiS_2 to achieve a high energy density. Previously, Rouxel et al. have systematically investigated the electronic structure of TiS_2 and $LiTiS_2$ using ex situ X-ray absorption spectroscopy (XAS) with a focus mainly on the sulfur K-edge, accompanied by multiple-scattering and band structure calculations.[25−27] The results unraveled that the lithium intercalation can induce the structural changes and the partial filling of the sulfur t_{2g} levels of TiS_2. However, an unambiguous understanding of the electronic and structural evolution of the TiS_2 electrode during the lithium interaction and conversion process under real operating conditions, which is still missing so far, highly relies on in situ and operando characterization methodologies.[28,29] Solving these issues is not only of great importance for the practical application of TiS_2 but also necessary for the further design of novel TMDs electrode materials with superior performance. In this report, we clearly elucidate the lithium intercalation and conversion reaction mechanism of the TiS_2 electrode in a lithium cell. We have applied ex situ and operando XAS combined with density functional theory (DFT) calculations to investigate the structural and chemical properties of TiS_2 during the lithiation−delithiation process to understand the electrochemical reaction mechanism. The advantage of synchrotron-based XAS methods is that it is chemically and elementally sensitive, and therefore it has been widely applied to investigate the local environment and oxidation state of selected elements.[30] By applying both qualitative and quantitative analyses of sulfur K-edge, Ti L-edge and K-edge, and O K-edge XAS results, we have demonstrated new insights into the cationic and anionic electrochemical activity and the dynamic behavior of the solid electrolyte interphase (SEI) of the TiS_2 electrode.

Results and Discussion. *Electrochemical Performance of TiS_2 Electrodes.* The electrochemical properties of TiS_2 were evaluated using a half-cell configuration in the voltage ranges of 1.4−3.0 V and 0.05−3.0 V versus Li/Li^+ at a current density of 200 mA/g. On the basis of previous reports, the intercalation reaction should take place for the former,[7,18,31] while both intercalation and conversion reactions should occur for the latter.[19,20] Figure 1a displays typical galvanostatic discharge/charge voltage profiles of TiS_2 with a discharge cutoff voltage of 1.4 V. The observation of monotonous behavior of the discharge/charge curves indicates a single-phase reaction during lithium intercalation/deintercalation. The TiS_2 electrode delivers an initial discharge and charge capacity of 208.8 and 190.2 mAh/g, respectively, corresponding to a Coulombic efficiency (CE) of 91.1% (Figure 1b). The relatively low CE could be related to electrolyte decomposition and/or the formation of a SEI film.[14,21] The cyclic voltammogram (CV) curves demonstrate several cathodic/anodic couples (Figure S1a), indicating a multistep lithiation/delithiation processes with the formation of a wide range of solid solutions of Li_xTiS_2 ($0 < x < 1$).[3,26] In addition, the reversible capacity is still maintained at 182.6 mAh/g with a CE higher than 99.9% after 100 cycles (Figure 1b), which renders the TiS_2 electrode an excellent candidate for reversible lithium storage.

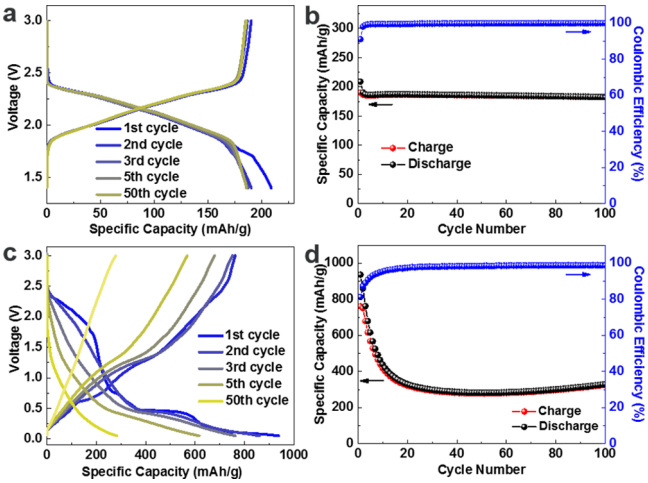

Figure 1. (a) Discharge/charge voltage profiles, (b) cycling performance and Coulombic efficiency of TiS_2 electrodes with a discharge cutoff voltage of 1.4 V. (c) Discharge/charge voltage profiles, (d) cycling performance and Coulombic efficiency of TiS_2 electrodes with a discharge cutoff voltage of 0.05 V. The specific current is 0.2 A/g.

Upon decreasing the discharge cutoff voltage to 0.05 V, the discharge voltage profile shows an additional plateau at ∼0.45 V (Figure 1c), corresponding to the conversion reaction of the TiS_2 electrode ($LiTiS_2 + 3Li^+ + 3e^- \rightarrow 2Li_2S + Ti$). The first discharge capacity is 936.4 mAh/g, which is close to the theoretical value of 960 mAh/g. However, a capacity of only 761.1 mAh/g is obtained after first charge probably due to the kinetic limitations in the charge process.[32] The conversion plateau is still visible in the second discharge process, suggesting the reversibility of the conversion reaction during the initial cycles. With further cycling the TiS_2 electrode, the conversion plateau gradually disappears, which is consistent with the CV results (Figure S1b). As a consequence, the reversible capacity decays to only 325.9 mAh/g after 100 cycles (Figure 1d). Note that the goal of the present study was to fundamentally understand the electrochemical reaction mechanism between TiS_2 and lithium; we therefore did not focus on electrode optimization and electrochemical performance improvement. Overall, the electrochemical performance of TiS_2 demonstrates a strong dependence on the discharge cutoff voltage and thus a fundamental understanding of the voltage-dependent reaction mechanism is needed.

Operando XAS of TiS_2 Electrodes in the Voltage Range of 1.4−3.0 V. We first investigated the intercalation reaction mechanism of TiS_2 by measuring the operando sulfur and Ti K-edge XAS spectra in the voltage range of 1.4−3.0 V. Figure 2a,b shows the representative operando Ti K-edge XAS spectra collected during the first discharge and charge processes, respectively. The total operando XAS spectra can be found in Figure S2. The transition metal K-edge XAS is a powerful tool to detect the oxidation state and site symmetry of the studied elements, which has been successfully applied in the past to investigate the charge storage mechanism of various transition metal oxides.[29,33−35] For the Ti K-edge XAS spectrum of pristine TiS_2, it shows a relatively weak pre-edge peak at ∼4970.0 eV and a strong absorption peak at ∼4989.0 eV. The pre-edge peak is attributed to the 1s to 3d transition, which is dipole forbidden for absorbers in a centrosymmetric environment.[33,34,36] The appearance of the weak pre-edge peak suggests the slightly distorted octahedral symmetry of Ti

DOI: 10.1021/acs.nanolett.8b01680
Nano Lett. XXXX, XXX, XXX−XXX

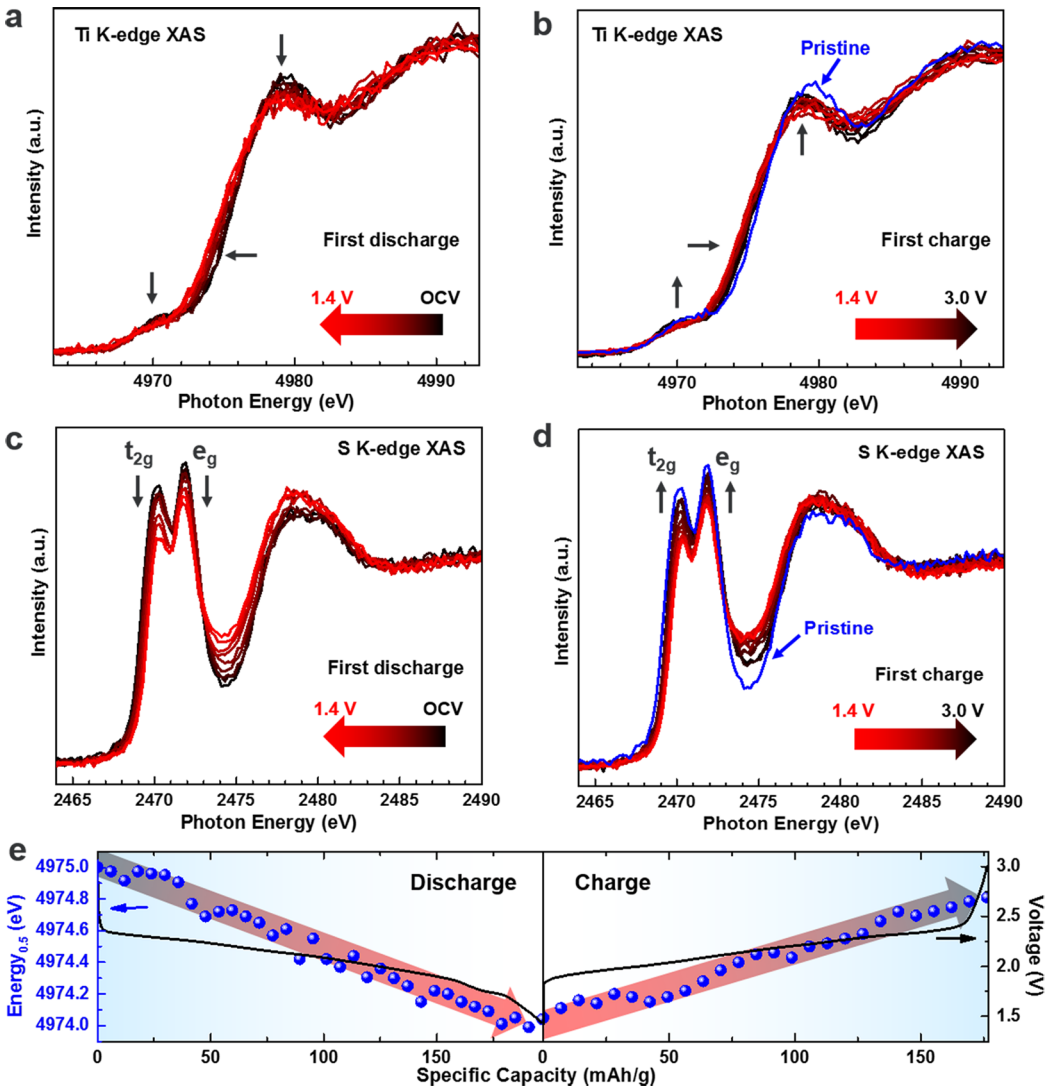

Figure 2. Operando XAS of TiS_2 electrodes in the voltage range of 1.4−3.0 V at a specific current of 0.05 A/g. Representive operando Ti K-edge (a) and sulfur K-edge (c) XAS spectra for the first discharge process. Representive operando Ti K-edge (b) and sulfur K-edge (d) XAS spectra for the first charge process. (e) Variation of Ti K-edge energy (at half height of normalized XAS spectra) as a function of specific capacity. The discharge−charge voltage profiles for the operando XAS measurement are also shown. The pristine Ti and sulfur XAS spectra were measured before the electrochemical process of the TiS_2 electrode.

atoms in the pristine TiS_2. The main absorption peak is caused by the dipole allowed transition of 1s to 4p orbitals. Because the outer p orbitals are more sensitive to the electronic structure change, we can estimate the average oxidation state of the measured metal atoms from the main absorption edge position. As the oxidation state of the metal atoms decreases, the main absorption edge shifts to lower energies and vice versa.[33,34,36]

During the first discharge process, the intensity of the pre-edge peak gradually decreases, indicating the local environment of Ti atoms gets more symmetrical as a nonsymmetrical octahedral environment will result in a higher intensity of the pre-edge peak.[33,37] This observation could be related to the strong repulsive interaction between inserted lithium ions and transition metal cations in the TiS_2 structure.[36] Note that the lattice expansion of TiS_2 induced by lithium intercalation may also lead to the suppression of the pre-edge peak. In addition, the intensity of the main absorption peak progressively decreases and the absorption edge shifts almost linearly toward lower energies (Figure 2e), reflecting a decrease of the average Ti oxidation state. During the charge process from 1.4 to 3.0 V, the absorption edge gradually shifts back to higher energies followed by an intensity increase due to the reoxidation of Ti (Figure 2e). A similar observation for the second cycle (Figure S3) indicates a high reversibility of the intercalation reaction, in good agreement with the superior cycling performance of TiS_2 electrode with a discharge cutoff voltage of 1.4 V. It should be mentioned that the slight deviation of the absorption edge energy from the linear change at the beginning and ending part of the discharge/charge process could be related to the change of the polarization and internal resistance of the electrode material. Note that the spectrum at the end of the first charge is not fully recovered to that of pristine TiS_2. This implies that the lithium ions are not totally deintercalated during charging probably owing to the kinetics of lithium release, which is consistent with the low Coulombic efficiency of the first cycle shown in Figure 1b.

To gain more insight into the variation of Ti oxidation state, we have quantified the valence state evolution of Ti by comparing the average oxidation state and the main absorption edge position at half height of Ti K-edge XAS spectra for TiS_2

DOI: 10.1021/acs.nanolett.8b01680
Nano Lett. XXXX, XXX, XXX−XXX

at different states of charge and titanium oxides, as demonstrated in Figure S4. On the basis of the linear relationship between the edge position and average oxidation state, the nominal Ti oxidation state of TiS_2 is estimated to be +2.7 rather than +4 due to the covalent bonds between Ti and sulfur.[8] During the first cycle, the average oxidation state change of Ti is −0.18 for the discharge and +0.15 for the charge. The interesting point is that the Ti oxidation state should decrease/increase by 0.81/0.73 with lithium intercalation/deintercalation if only Ti participates the redox reaction, as anticipated from the corresponding discharge/charge capacity (Figure 2e). The deviation of the Ti oxidation state change may indicate that not only Ti but also sulfur is involved in the redox reaction during cycling.

To further understand the lithium intercalation mechanism, we also calculated the structure of TiS_2 and $LiTiS_2$, as shown in Figure 3a,b. The results indicate that the lithium ions prefer to locate on the tetrahedral sites on top of Ti atoms, leading to a 10% expansion in the crystalline lattice along the direction perpendicular to the basal plane (5.68 Å for TiS_2 versus 6.18 Å for $LiTiS_2$). For both TiS_2 and $LiTiS_2$, the structure demonstrates an octahedral 1T phase, indicating the absence of a phase transition during the lithium intercalation process.

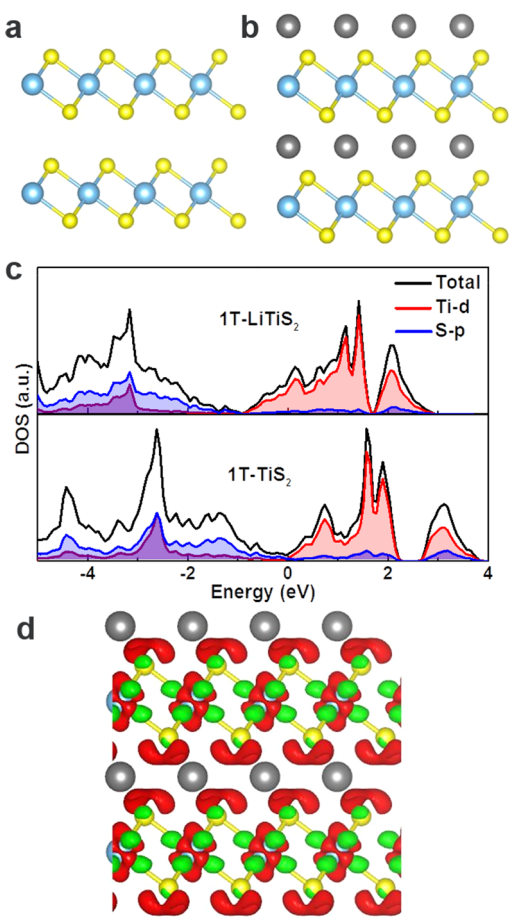

Figure 3. DFT calculations of the structure of TiS_2 before and after lithium intercalation. (a) The structure of TiS_2. (b) The structure of $LiTiS_2$. The gray, blue, and yellow balls represent Li, Ti and sulfur atoms, respectively. (c) Calculated density of states of TiS_2 and $LiTiS_2$. The Fermi energy is set at 0 eV. (d) Simulated charge-density distribution of TiS_2 after lithium intercalation, where the red and green regions indicate charge accumulation and depletion, respectively.

This is consistent with the single-phase transformation from TiS_2 to $LiTiS_2$ observed in the electrochemical process. In addition, the analysis of density of states (Figure 3c) reveals that both TiS_2 and $LiTiS_2$ exhibit a metallic character, which is responsible for the fast electron transport rate and thus the high charge/discharge rate capability.[15] Furthermore, we calculated the charge-density distribution of TiS_2 after lithium intercalation (Figure 3d). According to the Bader charge analysis, the charge on Ti and sulfur atoms are +1.504 e and −0.752 e for TiS_2, while these values change to +1.415 e and −1.136 e for $LiTiS_2$. As a consequence, the Ti and sulfur atoms get 0.089 and 0.384 e from each intercalated Li atom. The observation of charge accumulation around sulfur and Ti atoms for $LiTiS_2$ clearly demonstrates the charge transfer from lithium to both Ti and sulfur, suggesting that sulfur is also involved in the redox process during lithium intercalation.[38]

In order to further verify this hypothesis, we also recorded the operando sulfur K-edge XAS spectra for the first discharge and charge processes (Figure 2c,d). For the spectrum of pristine TiS_2, the two features located between 2469 and 2474 eV are induced by the strong hybridizations between Ti 3d and sulfur 3p states and can be assigned to the transitions to t_{2g} and e_g bandlike states, respectively;[25,26] the broad feature at ∼2480 eV is induced by the hybridization between sulfur 3p states and Ti 4s and 4p states. Upon lithium intercalation, the intensity of t_{2g} and e_g states decreases continuously (Figure 2c and Figure S5), which can be attributed to the partial filling of the t_{2g} states by electrons transferred from lithium and therefore the reduced transition probability of sulfur 1s to these levels during the absorption process.[26,27] In contrast, the broad feature at ∼2480 eV shows a progressive shift toward lower energies and an intensity increase in the discharge process because of the change of coordination number of sulfur atoms and the lithium−sulfur interaction as derived from full multiple-scattering theory.[26] The involvement of anionic redox for TiS_2 during lithium intercalation/delithiation process could be partially attributed to the overlap of the sulfur 3p states with the Ti 3d states (Figure 3c). It is notable that the anionic redox does not occur in TiO_2 because the oxygen 2p states have a lower energy than the sulfur 3p states, which results in less overlap with the Ti 3d states.[39] Upon charging, the intensity of t_{2g} and e_g states is largely recovered (Figure 2d and Figure S5), indicating the high reversibility of the lithium intercalation/deintercalation process as observed in the operando Ti K-edge XAS results. In summary, our operando XAS measurement clearly reveals the high electronic and structural reversibility of the TiS_2 electrode during lithium intercalation and deintercalation processes over the voltage range from 1.4 to 3.0 V, which is consistent with the excellent electrochemical performance shown above. In addition, we elucidate that the electrons transferred from intercalated lithium are not only located at the Ti 3d states but also the sulfur 3p states. In other words, sulfur is also electrochemically active and involved in the redox reaction during the lithium intercalation/deintercalation process.

Operando XAS of TiS_2 Electrodes in the Voltage Range of 0.05−3.0 V. As a next step, we investigated the conversion reaction mechanism of TiS_2 by decreasing the discharge cutoff voltage to 0.05 V. Figure 4 shows the representive operando Ti (a,b) and sulfur (c,d) K-edge XAS spectra during the discharge and charge processes, respectively. The total operando Ti and sulfur K-edge XAS spectra are displayed in Figure S6. The operando Ti K-edge XAS spectra (Figure 4a) show a

DOI: 10.1021/acs.nanolett.8b01680
Nano Lett. XXXX, XXX, XXX−XXX

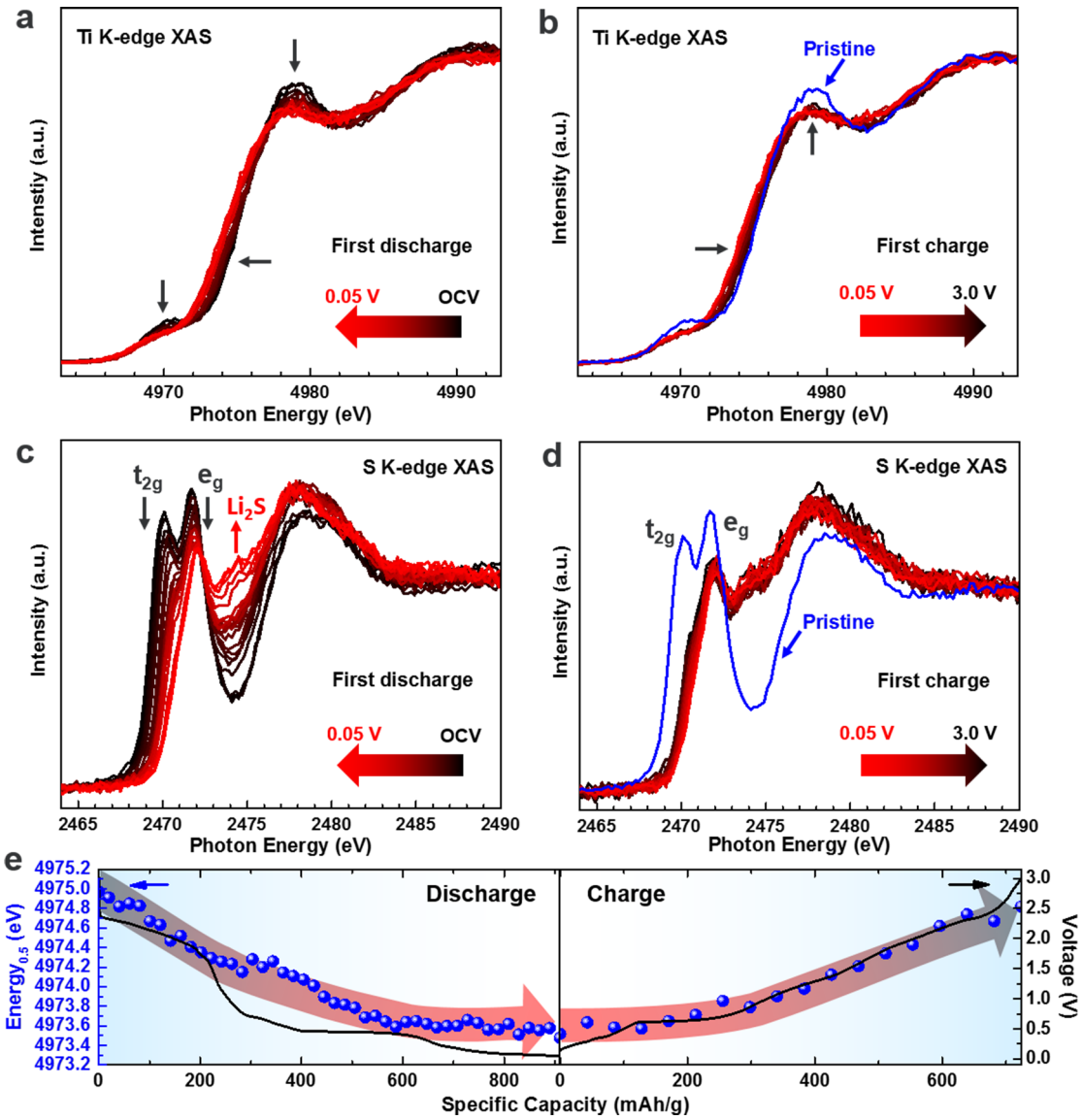

Figure 4. Operando XAS of TiS_2 electrodes in the voltage range of 0.05−3.0 V at a specific current of 0.2 A/g. Representive operando Ti K-edge (a) and sulfur K-edge (c) XAS spectra for the first discharge process. Representive operando Ti K-edge (b) and sulfur K-edge (d) XAS spectra for the first charge process. (e) Variation of Ti K-edge energy (at half height of normalized XAS spectra) as a function of specific capacity. The discharge−charge voltage profile during the operando XAS measurement is also shown. The pristine Ti and sulfur XAS spectra were measured before the electrochemical process of the TiS_2 electrode.

continuous intensity decrease of the pre-edge peak and a gradual downward shift of the 1s to 4p absorption edge accompanied by an intensity decrease during the first discharge process. These results indicate an increase of the local symmetry and a decrease in the average oxidation state of Ti,[33,37] which is similar to the behavior of the lithium intercalation reaction of TiS_2. The formation of Li_2S and metallic Ti is proposed for a full conversion reaction of TiS_2 after discharge to 0.05 V.[40] During the subsequent charge to 3.0 V, the Ti absorption edge gradually shifts back to higher energies and the intensity of the main absorption peak also increases, suggesting the oxidation of Ti ions during the charge process. However, the pre-edge peak is not recovered at the end of charge compared with the spectrum of pristine TiS_2, indicative of the partial irreversible structure change in the first cycle. This observation may be related to the energy barrier for Li_2S oxidation[41,42] and/or the amorphization of the TiS_2 electrode during the first cycle.[43] A similar phenomenon was also observed for other conversion electrodes in LIBs, for example, NiO,[32] MoS_2,[44] and VS_4.[45]

In order to visualize more clearly how the operando Ti K-edge XAS spectra are developed during the discharge and charge processes, we have plotted the Ti K-edge absorption edge energy as a function of specific capacity of the first cycle along with the discharge and charge voltage profiles for the operando XAS measurement, as shown in Figure 4e. During the first discharge from open circuit voltage (OCV) to 0.05 V, the edge energy shifts to lower energies linearly at the intercalation plateau and then slowly decreases at the conversion plateau and finally becomes almost constant at the end of the conversion plateau. The decreased energy change of the conversion plateau compared with that of the intercalation plateau could be related to the sluggish kinetics of the formation of the insulating Li_2S. However, the nominal oxidization state of Ti at the very end of

DOI: 10.1021/acs.nanolett.8b01680
Nano Lett. XXXX, XXX, XXX−XXX

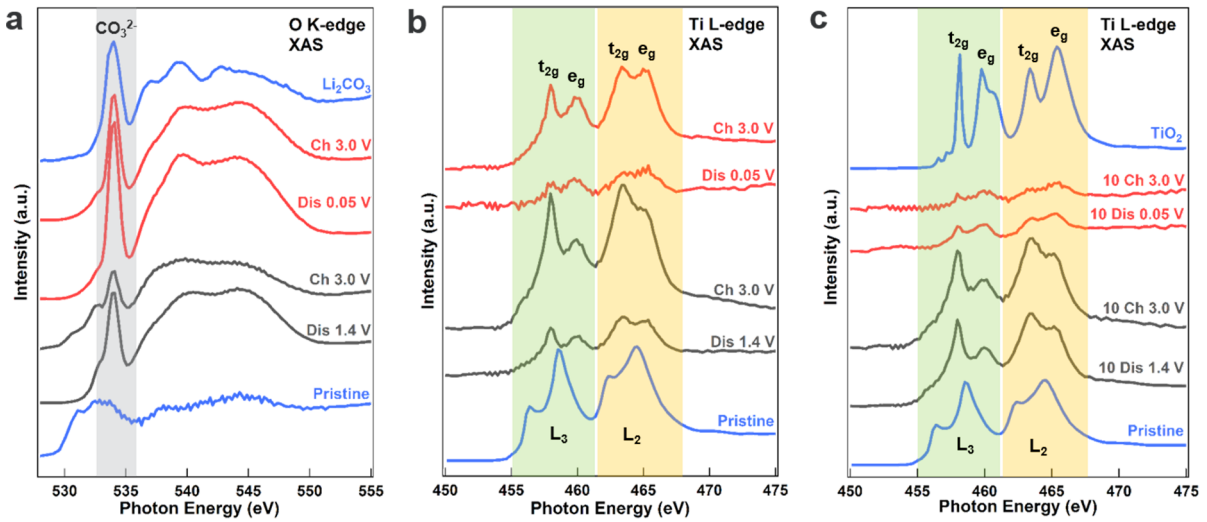

Figure 5. (a) Ex situ O K-edge XAS spectra of TiS_2 electrodes at different states of charge as labeled. (b) Ex situ Ti L-edge XAS spectra of TiS_2 electrodes at different states of charge as labeled. (c) Ex situ Ti L-edge XAS spectra of TiS_2 electrodes with different discharge cutoff voltages after 10 cycles. The spectra were recorded using surface-sensitive TEY mode.

first discharge (+2.39, see Figure S7) is higher than that of Ti metal. This could be induced by the strong interaction between the as formed Li_2S and Ti (Figure S8), which results in the charge transfer from Ti to Li_2S, and as a consequence the oxidation state of Ti is higher than that of Ti metal. During the following charge from 0.05 to 3.0 V, the edge energy shows a weak function of capacity initially and then gradually shifts to higher energies linearly, in accordance with the charge voltage profile. These results clearly demonstrate the reversible reduction/oxidation of Ti during the discharge/charge process, which is partially responsible for the high specific capacity of the first cycle.

Next, we measured the operando sulfur K-edge XAS spectra to better understand the conversion reaction mechanism of the TiS_2 electrode (Figure 4c,d). The intensity of t_{2g} and e_g states displays a continuous decrease during the discharge process (Figure 4c and Figure S9), and simultaneously, a broad feature at ~2475 eV is developed, which is attributed to the transformation from TiS_2 to Li_2S.[46,47] However, at the very end of discharge, the position of the Li_2S feature and the overall spectral shape are different from that of pure Li_2S,[44−46] which is related to the strong interaction between the as formed Li_2S and Ti as discussed above. Upon charging, the operando sulfur XAS spectra (Figure 4d and Figure S9) show a weak function of capacity, and the fingerprint feature of TiS_2 is not recovered at the end of charge. A similar phenomenon is also observed for the second cycle, as demonstrated in Figure S10. To better unravel the mechanism underpinning this observation, we have also performed ex situ sulfur K-edge XAS study for the cycled TiS_2 electrodes at different states of charge and the corresponding results are shown in Figure S11. It is clearly demonstrated that the characteristic t_{2g} and e_g features of TiS_2 are recovered for the electrode charged from 0.05 to 3.0 V, indicating at least partial reversibility of the conversion reaction for TiS_2. The weak real-time response of operando sulfur K-edge XAS to electrochemical cycling is most likely due to the electric insulating properties of the formed Li_2S, which means that the electrode in the operando condition is in a nonequilibrium state and a long relaxation time is necessary for the reformation of TiS_2. In contrast, the electrode for the ex situ measurement is in an equilibrium state due to the enough relaxation time.[48] Note that no such sluggish response is observed for the intercalation reaction of TiS_2 because of the high conductivity of the reaction products.

The reversibility of the conversion reaction for different electrodes in LIBs has been extensively investigated previously.[49−51] For example, the conversion reaction is CuF_2 is irreversible due to the direct oxidation of Cu into a soluble phase in the reconversion process,[47] whereas for FeF_2 the conversion reaction is highly reversible.[49] For a more closely related electrode of MoS_2, the conversion reaction is not reversible and the formed Li_2S is converted to sulfur in the subsequent charge process.[42,48] In order to have an in-depth understanding of the conversion reaction mechanism of TiS_2, we have calculated and compared the formation energy of different reaction paths (Figure S12). The formation energy for the conversion reaction of TiS_2 is −4.414 eV whereas this value decreases to −8.458 eV for that of sulfur/Li_2S, clearly indicating that the formed Li_2S is more thermodynamically favorable to convert back to TiS_2 rather than elemental sulfur during the charge process. Even though our DFT calculations were unable to simulate the kinetic behavior of the different reaction pathways, they did provide some computational support to understand the reversibility of the conversion reaction of TiS_2.

Surface Reaction and Capacity Degradation Mechanism of TiS_2 Electrodes. Having clarified the intercalation and conversion reaction mechanism, we now focus on the surface reaction and capacity fading mechanism of the TiS_2 electrode by measuring ex situ O K-edge and Ti L-edge XAS. It should be noted that these XAS spectra were recorded using total electron yield (TEY) mode, which is surface sensitive with a detection depth of up to 10 nm. Therefore, the XAS spectra recorded in TEY mode can exclusively measure the electronic properties of the SEI layer. Figure 5a shows the O K-edge XAS spectra collected from TiS_2 electrodes at different states of charge. The peak at 533.9 eV is the fingerprint feature of carbonate (CO_3^{2-}) species, while the shoulder feature at 532.4 eV originates from other organic compounds, for example, oxalate and/or −OH functional groups.[52] Interestingly, the spectra show a strong voltage dependent evolution. Specifically, the intensity of carbonate groups increases from OCV to 1.4 V and decreases from 1.4 to 3.0 V. The same phenomenon is also observed for

DOI: 10.1021/acs.nanolett.8b01680
Nano Lett. XXXX, XXX, XXX−XXX

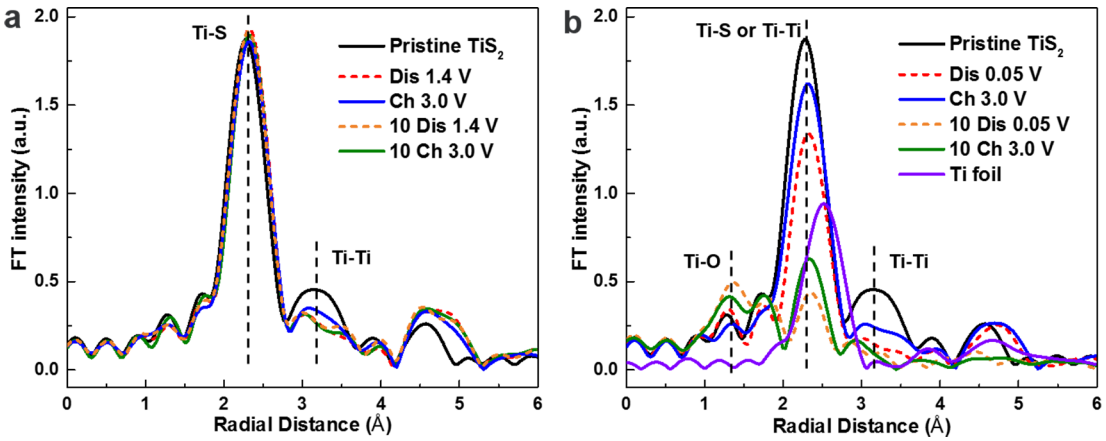

Figure 6. Ex situ Ti K-edge phase-corrected FT-EXAFS spectra of TiS_2 electrodes at different states of charge with a discharge cutoff voltage of 1.4 V (a) and 0.05 V (b), respectively.

the TiS_2 electrodes cycled between 0.05 and 3.0 V. The formation of carbonate species could be related to the electrochemical reaction between lithiated TiS_2 and carbonate-based solvents (EC and DEC) used in this study. It is worth mentioning that the intensity of carbonate related species is increased after discharging from 1.4 to 0.05 V, indicative of the further reduction of the carbonate solvents at lower discharge voltages. The reversible process for the development and partial decomposition of carbonate related species indicates the instability of the SEI layer formed on the electrode surface during the cycling process, which may result in capacity fading due to the continuous depletion of electrolyte. The dynamic alternation of the SEI layer upon charging and discharging is further verified by ex situ Raman results, as displayed in Figure S13. All these results suggest that the formation of the SEI layer on the surface of TiS_2 electrode is a highly dynamic process, which is in contrast to the conventional wisdom that the SEI layer is stable over long periods once it is formed.[53]

In addition to O K-edge XAS, we also measured Ti L-edge XAS to better understand the evolution of the SEI layer upon electrochemical cycling. The advantage of Ti L-edge XAS is that it can directly probe the Ti 3d oxidation states and chemical bonds through the 2p to 3d transitions. Figure 5b shows the Ti L-edge XAS spectra of TiS_2 electrodes at different states of charge. The spectra demonstrate two sets of features located at the ranges of 455−462 and 462−468 eV, respectively, which correspond to the L_3-edge and L_2-edge. The splitting of two absorption edges originates from the core-hole coupling effect. Each L-edge feature consists of t_{2g} and e_g peaks due to the crystal-field splitting of the Ti 3d orbitals. The L_2-edge feature is normally broadened compared with the L_3-edge feature because of the shorter lifetime of the $2p_{1/2}$ core hole and the near-threshold Coster−Kronig decay.[30] We therefore mainly focus on the L_3-edge evolution in the following discussions.

The L_3-edge XAS displays a strong evolution of both intensity and line shape upon electrochemical cycling. In particular, the XAS signal is partially suppressed for the electrodes discharged to 1.4 and 0.05 V and greatly enhanced after being charged back to 3.0 V. This observation suggests that the SEI layer is developed and partially decomposed during the discharge and charge processes, which is consistent with the breathing behavior of the SEI layer derived from O K-edge XAS results. The decrease during discharge and increase during charge of the t_{2g}/e_g intensity ratio corresponds to the reduction and oxidation of Ti ions, respectively, in accordance with the operando Ti K-edge XAS results. Interestingly, the spectral shape of the TiS_2 electrodes charged back to 3.0 V is still quite different from that of the pristine one, which could be related to the structural variation of TiS_2 due to the presence of residual lithium ions and thus the hybridization strength between Ti and sulfur, as observed in the operando Ti K-edge XAS.

Figure 5c shows the Ti L-edge XAS spectra of the TiS_2 electrodes at fully discharged (1.4 or 0.05 V) and charged (3.0 V) states after 10 cycles. Different from the behavior of the first cycle, the intensities of the t_{2g} and e_g peaks show only a minor change during discharge and charge of the 10th cycle because of the cover of the SEI layers with a similar thickness on the electrode surfaces. This indicates that the carbonate species in the SEI layer gradually lose their electrochemical activity with increasing cycle number and eventually become inactive, and therefore, the thickness of the SEI layer reaches a constant value. In addition, for the fully charged electrodes, the spectral intensity of the electrode with a discharge cutoff voltage of 0.05 V is lower than that of 1.4 V, a strong indication of the formation of a thicker SEI layer for the former. Moreover, the spectral shape, especially the t_{2g}/e_g intensity ratio, of the electrodes cycled between 0.05 and 3.0 V becomes somewhat similar to that of TiO_2, which may suggest the formation of chemical bonds between conversion reaction product Ti and oxygen containing fragments (most likely decomposed solvents). This hypothesis is plausible considering the high activity of as-formed Ti clusters at deep discharge and the higher electronegativity of oxygen compared with that of sulfur.[54,55] The formation of Ti—O related compounds during the cycling process could decrease the reversibility of the conversion reaction of TiS_2, which may be partially responsible for the rapid capacity fading as shown in Figure 1d.

We further performed Ti K-edge extended X-ray absorption fine structure (EXAFS) experiments to gain more insight into the capacity degradation mechanism of TiS_2 electrodes. Figure 6 shows the Fourier-transformed (FT) curves of the Ti K-edge EXAFS spectra at different states of charge in the voltage ranges of 1.4−3.0 V (a) and 0.05−3.0 V (b). The corresponding k^2-weighted EXAFS $\chi(k)$ spectra are shown in Figure S14. The FT curve of the pristine TiS_2 electrode exhibits a prominent feature at 2.3 Å, which is unambiguously ascribed to Ti—S coordination. In contrast, the peak at 3.2 Å arises from the nearest Ti—Ti coordination and the peak at 4.6 Å is the

DOI: 10.1021/acs.nanolett.8b01680
Nano Lett. XXXX, XXX, XXX−XXX

contribution of the focused multiscattering arising from the Ti—Ti—Ti triplet linear relation due to the planar layer structure of TiS_2.[56] For the TiS_2 electrodes cycled between 1.4 and 3.0 V, the amplitude of the Ti—S bond almost remains the same even after 10 cycles, indicating the minor structural change of the electrodes during electrochemical cycling. This observation is consistent with the excellent cycling performance of TiS_2 in the voltage range of 1.4–3.0 V. Note that the amplitude of Ti—Ti bond slightly decreases for TiS_2 discharged to 1.4 V and does not fully recover after being charged back to 3.0 V, which might be related to the slight irreversible local structural change due to the remaining lithium ions and the possible displacement of Ti ions into less symmetric environments.[34]

In contrast, dramatic change is observed for the TiS_2 electrodes cycled between 0.05 and 3.0 V, especially for the Ti—S coordination. As discharged to 0.05 V, the amplitude of Ti—S coordination markedly decreases and the peak position shifts slightly to higher *R* value. To exclude the possibility that the TiS_2 electrode is not fully converted, we also measured X-ray diffraction (XRD) for the electrode discharged to 0.05 V (Figure S15). It is clearly shown that the characteristic diffraction pattern of TiS_2 totally vanishes and instead the corresponding pattern of Li_2S is developed, strongly indicating the complete conversion from TiS_2 to Li_2S. No diffraction pattern related to metallic Ti is observed probably due to the small size of the formed Ti clusters, which has also been observed for other conversion electrodes, like NiO,[32] FeF_2,[50] and MoS_2.[43] Therefore, the observed feature at 2.3 Å is more likely attributable to the Ti—Ti coordination of formed Ti clusters rather than the unreacted TiS_2. However, the bonding length is shorter than that of Ti foil, which is possibly related to the strong interaction between the as formed Ti clusters and Li_2S, as discussed above. During subsequent charging up to 3.0 V, the amplitude of Ti—S coordination rises, manifesting the partial reversibility of the conversion reaction of TiS_2 in the first cycle. Notably, upon discharge to 0.05 V after 10 cycles, the intensity of the peak at 2.3 Å significantly drops and a new feature at 1.4 Å is developed. According to the position, the newly formed feature can be attributed to Ti—O coordination,[57] indicating the formation of Ti—O related compounds during the extended cycling process, as observed in the Ti L-edge XAS results. Note that the amplitude of the Ti—O coordination is comparable to that of the peak at 2.3 Å, which suggests that both the surface and bulk Ti species of the TiS_2 electrode are involved in the formation of Ti—O compounds. The amplitude of the Ti—S coordination only shows a slight increase after charging back to 3.0 V. This implies that the formed Ti—O related compounds are not converted back to TiS_2 in the charge process, which results in the decreased reversible capacity.

Conclusions. We have applied ex situ and operando X-ray absorption spectroscopy experiments combined with DFT calculations to investigate the electronic and structural evolution of the TiS_2 electrodes to comprehensively understand the electrochemical reaction mechanism. The intercalation reaction of TiS_2 is highly reversible, which renders a high reversible specific capacity of 182.6 mAh/g after 100 cycles. During the intercalation process, the transferred electrons are located not only on the Ti 3d orbitals but also on the sulfur 3p orbitals, indicating that both Ti and sulfur are involved in the redox process for the intercalation. In contrast, the conversion reaction of TiS_2 is only partially reversible in the first discharge–charge process. With further cycling of the electrode, Ti—O related compounds are developed due to the high reactivity of the as formed Ti metal clusters and the higher electronegativity of oxygen compared with that of sulfur, which results in the decreased reversibility of the conversion reaction and fast capacity fading. In addition, the formation of the SEI layer on the surface of TiS_2 electrode is a highly dynamic process with the development and partial decomposition of carbonate related species in the SEI layer during the discharge and charge processes, respectively. Upon further cycling, the formed carbonates in the SEI layer gradually lose electrochemical activity and finally become mature. Our present study delivers new insights into the electrochemical reaction mechanism of the TiS_2 electrode, which are crucially important for the further optimization of layered TMD electrode composites and manufacturing methods to achieve superior electrochemical performance. Additionally, the operando methods applied in this study can also be extended to investigate the electrochemical reaction mechanism of TiS_2 electrodes in other rechargeable battery systems, for example, potassium ion batteries[58] and magnesium ion batteries.[59,60]

Experimental and Calculation Details. *Cell Preparation and Electrochemical Cycling.* The TiS_2 electrodes were prepared by grinding a mixture containing the commercial TiS_2 active material (Sigma), carbon black (superP) and polyvinylidene fluoride (PVDF) (pure TiS_2/C/PVDF = 70:20:10, by weight) for 10 min, then dispersing the mixture in *N*-methyl-2-pyrrolidinone (NMP) to make a slurry with a concentration of 300 mg/mL and stirring for 4 h, coating the slurry onto a commercial copper foil and evaporating the solvent at room temperature inside of a glovebox (filled with argon) and drying overnight. One molar $LiPF_6$ in ethylene carbonate (EC)/diethyl carbonate (DEC) (1:1, by volume) was used as electrolyte. CR2325 coin cells were assembled in an argon-filled glovebox. The cell consisted of a fabricated TiS_2 electrode, a lithium metal foil electrode and a porous polypropylene separator (Celgard 2400). The electrochemical performance of the cells was evaluated between 1.4 and 3.0 V or 0.05 and 3.0 V using a battery cycler (Arbin BT2000). The CV study was conducted using a Biologic electrochemical workstation using Li/Li^+ as a reference at a scan rate of 0.05 mV/s.

X-ray Absorption Spectroscopy Measurements. The in situ/operando and ex situ sulfur K-edge XAS spectra were measured at beamline 5.3.1 at the Advanced Light Source (ALS), Lawrence Berkeley National Laboratory (LBNL). The X-ray beam size is ~100 μm × 100 μm. The XAS spectra were collected in total fluorescence yield mode and calibrated using elemental sulfur spectra by setting the position of the white line to 2472.2 eV. All the XAS spectra were measured under constant helium flow in the sample chamber and acquired continuously during the discharge/charge processes. The in situ electrochemical cells were adapted from the CR2325 coin cells: a 2 × 1 mm^2 hole was drilled at the TiS_2 (positive) side of the cell housing using a high precision laser system; the hole was then sealed with a 13 μm thick Kapton film to avoid air exposure while allowing X-ray beam penetration (the X-ray transmission ratio of a 13 μm thick Kapton film at 2470 eV is ~65%). In addition, we applied a copper mesh (Dexmet, 30% open area, 25 μm thick) as the holder for the TiS_2 electrode materials to allow the direct detection of TiS_2 by incoming X-rays. For the anode side, we just used the regular lithium foil because we measured the fluorescence rather than the

DOI: 10.1021/acs.nanolett.8b01680
Nano Lett. XXXX, XXX, XXX–XXX

transmission signal for the S and Ti K-edge XAS.[61] The ex situ Ti L-edge and O K-edge XAS spectra were measured at beamline 8.0.1.4 at the ALS, LBNL. The ex situ Ti K-edge EXAFS spectra were measured at beamline 16A1 of National Synchrotron Radiation Research Center, Taiwan (NSRRC). The analysis of EXAFS data was performed using the Artemis program.

Calculation Details. DFT calculations were performed using the Vienna ab initio simulation package (VASP).[62] The projector-augmented wave method[63] was used to describe the core−valence interaction. To account for the effect of van der Waals interaction, the optB86b-vdW functional was adopted as the exchange-correlation functional.[64] The wave functions are expanded in a plane-wave basis set with a 400 eV cutoff. All atoms are allowed to relax until the calculated force on each atom is smaller than 0.01 eV/Å. The primitive hexagonal cell of TiS_2 is used for the calculation. The optimized in-plane and out-of-plane lattice constants are 3.37 and 5.68 Å for TiS_2 and are 3.42 and 6.18 Å for $LiTiS_2$, respectively. A Gamma-centered 11 × 11 × 6 Monkhorst−Pack *k*-point mesh is used for structural relaxation and charge density calculation. The mesh is increased to 21 × 21 × 12 for DOS calculation. The Gaussian smearing method with a broadening of 0.05 eV is used to determine the eigenstate occupation.

■ ASSOCIATED CONTENT

Supporting Information

The Supporting Information is available free of charge on the ACS Publications website at DOI: 10.1021/acs.nanolett.8b01680.

Additional experimental and theoretical details. Figures showing cyclic voltammograms, ex situ and operando XAS analysis, XRD and Raman analysis, binding and formation energies (PDF)

■ AUTHOR INFORMATION

Corresponding Author

*E-mail: jguo@lbl.gov.

ORCID

Liang Zhang: 0000-0002-3446-3172
Elton J. Cairns: 0000-0002-1179-7591
Jinghua Guo: 0000-0002-8576-2172

Notes

The authors declare no competing financial interest.

■ ACKNOWLEDGMENTS

The work at Advanced Light Source of the Lawrence Berkeley National Laboratory were supported by the Director, Office of Science, Office of Basic Energy Sciences, of the U.S. Department of Energy under Contract No. DE-AC02-05CH11231. Work in the Energy Technologies Area of Lawrence Berkeley National Laboratory was supported by CERDEC U.S. ARMY under project No.104302. The work for the ab initio calculation was supported by Director, Office of Science, Office of Basic Energy Sciences, of the U.S. Department of Energy under Contract No. DE-AC02-05CH11231 through the theory of material (KC2301) program. It uses the resources of National Energy Research Scientific Computing (NERSC) center at Lawrence Berkeley National Laboratory.

■ REFERENCES

(1) Zhou, L.; Zhang, K.; Hu, Z.; Tao, Z.; Mai, L.; Kang, Y.-M.; Chou, S.-L.; Chen, J. *Adv. Energy Mater.* **2018**, *8*, 1701415.
(2) Liu, Y.; Zhou, G.; Liu, K.; Cui, Y. *Acc. Chem. Res.* **2017**, *50*, 2895−2905.
(3) Goodenough, J. B.; Park, K. S. *J. Am. Chem. Soc.* **2013**, *135*, 1167−1176.
(4) Tan, C.; Cao, X.; Wu, X. J.; He, Q.; Yang, J.; Zhang, X.; Chen, J.; Zhao, W.; Han, S.; Nam, G. H.; Sindoro, M.; Zhang, H. *Chem. Rev.* **2017**, *117*, 6225−6331.
(5) Zhang, Y.; Zhou, Q.; Zhu, J.; Yan, Q.; Dou, S. X.; Sun, W. *Adv. Funct. Mater.* **2017**, *27*, 1702317.
(6) Wang, T.; Chen, S.; Pang, H.; Xue, H.; Yu, Y. *Adv. Sci.* **2017**, *4*, 1600289.
(7) Whittingham, M. S. *Science* **1976**, *192*, 1126−1127.
(8) Tarascon, J.-M.; Armand, M. *Nature* **2001**, *414*, 359−367.
(9) Whittingham, M. S. *Chem. Rev.* **2004**, *104*, 4271−4302.
(10) Lin, D.; Liu, Y.; Cui, Y. *Nat. Nanotechnol.* **2017**, *12*, 194−206.
(11) Liang, X.; Pang, Q.; Kochetkov, I. R.; Sempere, M. S.; Huang, H.; Sun, X.; Nazar, L. F. *Nature Energy* **2017**, *2*, 17119.
(12) Zang, X.; Shen, C.; Kao, E.; Warren, R.; Zhang, R.; Teh, K. S.; Zhong, J.; Wei, M.; Li, B.; Chu, Y.; Sanghadasa, M.; Schwartzberg, A.; Lin, L. *Adv. Mater.* **2018**, *30*, 1704754.
(13) Whiteley, J. M.; Hafner, S.; Han, S. S.; Kim, S. C.; Le, V.-D.; Ban, C.; Kim, Y. H.; Oh, K. H.; Lee, S.-H. *J. Mater. Chem. A* **2017**, *5*, 15661−15668.
(14) Chaturvedi, A.; Hu, P.; Aravindan, V.; Kloc, C.; Madhavi, S. *J. Mater. Chem. A* **2017**, *5*, 9177−8181.
(15) Oh, D. Y.; Choi, Y. E.; Kim, D. H.; Lee, Y.-G.; Kim, B.-S.; Park, J.; Sohn, H.; Jung, Y. S. *J. Mater. Chem. A* **2016**, *4*, 10329−10335.
(16) Whittingham, M. S.; Gamble, F. R. *Mater. Res. Bull.* **1975**, *10*, 363−371.
(17) Gao, T.; Han, F.; Zhu, Y.; Suo, L.; Luo, C.; Xu, K.; Wang, C. *Adv. Energy Mater.* **2015**, *5*, 1401507.
(18) Trevey, J. E.; Stoldt, C. R.; Lee, S.-H. *J. Electrochem. Soc.* **2011**, *158*, A1282−A1289.
(19) Kartick, B.; Srivastava, S. K.; Mahanty, S. *J. Nanopart. Res.* **2013**, *15*, 1950.
(20) Chen, S.-Y.; Wang, Z.-X.; Fang, X.-P.; Zhao, H.-L.; Liu, X.-J.; Chen, L.-Q. *Acta Phys.-Chim. Sin.* **2011**, *27*, 97−102.
(21) Sun, W.; Suo, L.; Wang, F.; Eidson, N.; Yang, C.; Han, F.; Ma, Z.; Gao, T.; Zhu, M.; Wang, C. *Electrochem. Commun.* **2017**, *82*, 71−74.
(22) Vaccaro, A. J.; Palanisamy, T.; Kerr, R.; Maloy, J. *Solid State Ionics* **1981**, *2*, 337−340.
(23) Holleck, G.; Driscoll, J. *Electrochim. Acta* **1977**, *22*, 647−655.
(24) Chianelli, R.; Scanlon, J.; Rao, B. *J. Electrochem. Soc.* **1978**, *125*, 1563−1566.
(25) Wu, Z.; Lemoigno, F.; Gressier, P.; Ouvrard, G.; Moreau, P.; Rouxel, J.; Natoli, C. *Phys. Rev. B: Condens. Matter Mater. Phys.* **1996**, *54*, R11009.
(26) Wu, Z.; Ouvrard, G.; Lemaux, S.; Moreau, P.; Gressier, P.; Lemoigno, F.; Rouxel, J. *Phys. Rev. Lett.* **1996**, *77*, 2101.
(27) Moreau, P.; Ouvrard, G.; Gressier, P.; Ganal, P.; Rouxel, J. *J. Phys. Chem. Solids* **1996**, *57*, 1117−1122.
(28) Lu, J.; Wu, T.; Amine, K. *Nature Energy* **2017**, *2*, 17011.
(29) Huang, W.; Marcelli, A.; Xia, D. *Adv. Energy Mater.* **2017**, *7*, 1700460.
(30) Lin, F.; Liu, Y.; Yu, X.; Cheng, L.; Singer, A.; Shpyrko, O. G.; Xin, H. L.; Tamura, N.; Tian, C.; Weng, T. C.; Yang, X. Q.; Meng, Y. S.; Nordlund, D.; Yang, W.; Doeff, M. M. *Chem. Rev.* **2017**, *117*, 13123−13186.
(31) Li, T.; Liu, Y. H.; Chitara, B.; Goldberger, J. E. *J. Am. Chem. Soc.* **2014**, *136*, 2986−2989.
(32) Lin, F.; Nordlund, D.; Weng, T. C.; Zhu, Y.; Ban, C.; Richards, R. M.; Xin, H. L. *Nat. Commun.* **2014**, *5*, 3358.
(33) Deb, A.; Bergmann, U.; Cramer, S. P.; Cairns, E. J. *J. Electrochem. Soc.* **2007**, *154*, A534−A541.

DOI: 10.1021/acs.nanolett.8b01680
Nano Lett. XXXX, XXX, XXX−XXX

(34) Bak, S.-M.; Qiao, R.; Yang, W.; Lee, S.; Yu, X.; Anasori, B.; Lee, H.; Gogotsi, Y.; Yang, X.-Q. *Adv. Energy Mater.* **2017**, *7*, 1700959.
(35) Yang, Y.; Liu, X.; Dai, Z.; Yuan, F.; Bando, Y.; Golberg, D.; Wang, X. *Adv. Mater.* **2017**, *29*, 1606922.
(36) Zhou, D.; Permien, S.; Rana, J.; Krengel, M.; Sun, F.; Schumacher, G.; Bensch, W.; Banhart, J. *J. Power Sources* **2017**, *342*, 56−63.
(37) Yoon, W.-S.; Grey, C. P.; Balasubramanian, M.; Yang, X.-Q.; McBreen, J. *Chem. Mater.* **2003**, *15*, 3161−3169.
(38) Li, S. N.; Liu, J. B.; Liu, B. X. *J. Power Sources* **2016**, *320*, 322−331.
(39) Borghols, W. J. H.; Lützenkirchen-Hecht, D.; Haake, U.; Van Eck, E. R. H.; Mulder, F. M.; Wagemaker, M. *Phys. Chem. Chem. Phys.* **2009**, *11*, 5742−5748.
(40) Cabana, J.; Monconduit, L.; Larcher, D.; Palacin, M. R. *Adv. Mater.* **2010**, *22*, 170.
(41) Zhou, G. M.; Tian, H.; Jin, Y.; Tao, X.; Liu, B.; Zhang, R.; Seh, Z. W.; Zhuo, D.; Liu, Y.; Sun, J.; Zhao, J.; Zu, C.; Wu, D. S.; Zhang, Q.; Cui, Y. *Proc. Natl. Acad. Sci. U. S. A.* **2017**, *114*, 840−845.
(42) Zhou, G. M.; Sun, J.; Jin, Y.; Chen, W.; Zu, C.; Zhang, R.; Qiu, Y.; Zhao, J.; Zhuo, D.; Liu, Y.; Tao, X.; Liu, W.; Yan, K.; Lee, H. R.; Cui, Y. *Adv. Mater.* **2017**, *29*, 1603366.
(43) Sakuda, A.; Ohara, K.; Fukuda, K.; Nakanishi, K.; Kawaguchi, T.; Arai, H.; Uchimoto, Y.; Ohta, T.; Matsubara, E.; Ogumi, Z.; Okumura, T.; Kobayashi, H.; Kageyama, H.; Shikano, M.; Sakaebe, H.; Takeuchi, T. *J. Am. Chem. Soc.* **2017**, *139*, 8796−8799.
(44) Xiao, J.; Wang, X.; Yang, X.-Q.; Xun, S.; Liu, G.; Koech, P. K.; Liu, J.; Lemmon, J. P. *Adv. Funct. Mater.* **2011**, *21*, 2840−2846.
(45) Britto, S.; Leskes, M.; Hua, X.; Hebert, C. A.; Shin, H. S.; Clarke, S.; Borkiewicz, O.; Chapman, K. W.; Seshadri, R.; Cho, J.; Grey, C. P. *J. Am. Chem. Soc.* **2015**, *137*, 8499−8508.
(46) Zhang, L.; Sun, D.; Feng, J.; Cairns, E. J.; Guo, J. *Nano Lett.* **2017**, *17*, 5084−5091.
(47) Gorlin, Y.; Patel, M. U. M.; Freiberg, A.; He, Q.; Piana, M.; Tromp, M.; Gasteiger, H. A. *J. Electrochem. Soc.* **2016**, *163*, A930−A939.
(48) Zhang, L.; Sun, D.; Kang, J.; Feng, J.; Bechtel, H. A.; Wang, L. W.; Cairns, E. J.; Guo, J. *Nano Lett.* **2018**, *18*, 1466−1475.
(49) Stephenson, T.; Li, Z.; Olsen, B.; Mitlin, D. *Energy Environ. Sci.* **2014**, *7*, 209−231.
(50) Badway, F.; Mansour, A.; Pereira, N.; Al-Sharab, J.; Cosandey, F.; Plitz, I.; Amatucci, G. *Chem. Mater.* **2007**, *19*, 4129−4141.
(51) Wang, F.; Robert, R.; Chernova, N. A.; Pereira, N.; Omenya, F.; Badway, F.; Hua, X.; Ruotolo, M.; Zhang, R.; Wu, L.; Volkov, V.; Su, D.; Key, B.; Whittingham, M. S.; Grey, C. P.; Amatucci, G. G.; Zhu, Y.; Graetz, J. *J. Am. Chem. Soc.* **2011**, *133*, 18828−18836.
(52) Zhuo, Z.; Lu, P.; Delacourt, C.; Qiao, R.; Xu, K.; Pan, F.; Harris, S. J.; Yang, W. *Chem. Commun.* **2018**, *54*, 814−817.
(53) Peled, E.; Menkin, S. *J. Electrochem. Soc.* **2017**, *164*, A1703−A1719.
(54) Yu, S. H.; Lee, S. H.; Lee, D. J.; Sung, Y. E.; Hyeon, T. *Small* **2016**, *12*, 2146−2172.
(55) Park, K. H.; Choi, J.; Kim, H. J.; Oh, D. H.; Ahn, J. R.; Son, S. U. *Small* **2008**, *4*, 945−950.
(56) Reinhardt, F.; Beckhoff, B.; Eba, H.; Kanngiesser, B.; Kolbe, M.; Mizusawa, M.; Muller, M.; Pollakowski, B.; Sakurai, K.; Ulm, G. *Anal. Chem.* **2009**, *81*, 1770−1776.
(57) Liu, F.; He, H.; Xie, L. *ChemCatChem* **2013**, *5*, 3760−3769.
(58) Tian, B.; Tang, W.; Leng, K.; Chen, Z.; Tan, S. J. R.; Peng, C.; Ning, G.-H.; Fu, W.; Su, C.; Zheng, G. W.; Loh, K. P. *ACS Energy Lett.* **2017**, *2*, 1835−1840.
(59) Yoo, H. D.; Liang, Y.; Dong, H.; Lin, J.; Wang, H.; Liu, Y.; Ma, L.; Wu, T.; Li, Y.; Ru, Q.; Jing, Y.; An, Q.; Zhou, W.; Guo, J.; Lu, J.; Pantelides, S. T.; Qian, X.; Yao, Y. *Nat. Commun.* **2017**, *8*, 339.
(60) Sun, X.; Bonnick, P.; Nazar, L. F. *ACS Energy Lett.* **2016**, *1*, 297−301.
(61) Zhao, J.; Zhou, G. M.; Yan, K.; Xie, J.; Li, Y. Z.; Liao, L.; Jin, Y.; Liu, K.; Hsu, P.-C.; Wang, J. Y.; Cheng, H.-M.; Cui, Y. *Nat. Nanotechnol.* **2017**, *12*, 993−999.
(62) Kresse, G.; Furthmüller, J. *Phys. Rev. B: Condens. Matter Mater. Phys.* **1996**, *54*, 11169.
(63) Blöchl, P. E. *Phys. Rev. B: Condens. Matter Mater. Phys.* **1994**, *50*, 17953.
(64) Klimeš, J.; Bowler, D. R.; Michaelides, A. *Phys. Rev. B: Condens. Matter Mater. Phys.* **2011**, *83*, 195131.

DOI: 10.1021/acs.nanolett.8b01680
Nano Lett. XXXX, XXX, XXX−XXX